Duncan, R.A., Tarduno, J.A., Davies, T.A., and Scholl, D.W. (Eds.)
Proceedings of the Ocean Drilling Program, Scientific Results Volume 197

5. General-Purpose Inclinometry Modules in Highly Magnetized Formations: Are Borehole Wall Microresistivity Images Properly Oriented?[1]

P. Gaillot,[2,3] F. Einaudi,[3] J. Stoll,[4] and M. Leven[5]

ABSTRACT

Although magnetically oriented microresistivity borehole wall imaging tools were initially developed for weakly magnetized sedimentary formations, their scientific application to highly magnetized formations allows imaging of the in situ structure of oceanic crust. Quantitative structural interpretation of such images made during Ocean Drilling Program (ODP) Legs 118, 176, and 197 relies on their proper orientation. Using magnetic measurements, we investigated the influence of natural remanent magnetization (NRM) and magnetic susceptibility (MS) on tool orientation determination. Formations drilled in Hole 1203A during Leg 197 are characterized by alternating layers of basalts and volcaniclastic sediments having NRM in the range of 1–10 A/m and MS between 10^{-4} and 10^{-1} SI. Because it was logged with both the oriented Göttingen Borehole Magnetometer (GBM) and conventional (nonoriented general-purpose inclinometry capsule [GPIC] and tool [GPIT]) magnetometers, this data set provides a unique opportunity to test a filtering algorithm that isolates the rotational component of the tool by comparing the raw total magnetic field records with the tabulated geomagnetic field at this site. These results are validated by comparing the computed rotational component (magnetic-based tool rotation) with the direct (optical-gyro based) record of tool rotation as measured using the GBM. Using these data and the data recorded dur-

[1]Gaillot, P., Einaudi, F., Stoll, J., and Leven, M., 2004. General-purpose inclinometry modules in highly magnetized formations: are borehole wall microresistivity images properly oriented? *In* Duncan, R.A., Tarduno, J.A., Davies, T.A., and Scholl, D.W. (Eds.), *Proc. ODP, Sci. Results,* 197, 1–22 [Online]. Available from World Wide Web: <http://www-odp.tamu.edu/publications/197_SR/VOLUME/CHAPTERS/005.PDF>. [Cited YYYY-MM-DD]
[2]Laboratoire d'imagerie Géophysique, IPRA, Université de Pau et des Pays de l'Adour, 64000 PAU, France. Correspondence author: **philippe.gaillot@univ-pau.fr**
[3]Laboratoire de Géophysique et Hydrodynamique de Forage, ISTEEM, Université de Montpellier 2, Place Eugène Bataillon, CC056, 34095 Montpellier Cedex 5, France.
[4]Federal Institute of Geosciences and Natural Resources, Marine Geophysics Department, Stilleweg 2, 30655 Hannover, Germany.
[5]Institut für Geophysik, Universität Göttingen, Herzberger Landstrasse 180, 37075 Göttingen, Germany.

Initial receipt: 13 April 2004
Acceptance: 3 September 2004
Web publication: 10 December 2004
Ms 197SR-005

ing Leg 118 and in Leg 176 Hole 735B, which was drilled in gabbroic basement characterized by oxide-rich layers having NRM as high as 130 A/m and MS as high as 10^{-1} SI, we compare the previously validated algorithm to the Schlumberger algorithm traditionally used to compute the rotational component of the tool in sedimentary formations (NRM $\leq 10^{-1}$ A/m; MS < 10^{-4} SI). Provided that the oxide-rich layers are thin enough and separated by a distance large enough to produce only high-frequency fluctuations in the magnetic records, the rotational component of the tool can be obtained by both algorithms, validating the use of the standard Schlumberger algorithm for structural applications in such environments.

INTRODUCTION

For obvious economic reasons (exploration and exploitation of oil and gas), most logging tools, algorithms, and interpretative techniques were initially developed for sedimentary formations. In the framework of ocean drilling programs Deep Sea Drilling Project (DSD)) and Ocean Drilling Program (ODP), these technologies have been progressively applied to igneous and metamorphic ("hard rock") formations, tackling problems linked to oceanic crust internal structures (Goldberg, 1997; Ayadi et al., 1998; Brewer et al., 1998, 1999). In addition to traditional wireline logging tools (spectral gamma ray, lithodensity, electrical resistivity, porosity, acoustic velocities; see, for example, Rider, 1996), the Schlumberger Formation MicroScanner (FMS) and the Ultrasonic Borehole Imager (UBI) bring a new dimension to in situ characterization of penetrated formations (Serra, 1989; Pezard and Luthi, 1988; Pezard et al., 1988; Lovell et al., 1998). In the following discussion, we focus on the routinely used FMS-sonic tool string (**www.ldeo.columbia.edu/BRG/**), but an identical discussion is also valid for the UBI, which was recently deployed during ODP Leg 206 (Wilson, Teagle, Acton, et al., 2003).

The FMS is a probe with four orthogonal pads, each containing 16 microelectrodes (or buttons) of 6.5 mm radius. By measuring local microconductance of the formation, the electrodes provide a high-resolution resistivity image of the formation. Detection of resistivity contrasts allows identification of lithology changes, veins, fractures, and faults. When the image is "unrolled" and displayed from 0° to 360°, linear features intersecting the borehole appear as sinusoids (Rider, 1996). Assuming that FMS images are properly oriented to geographic north, the amplitude and minimum of the sinusoids can be related to the dip and azimuth of the associated feature, respectively, and, consequently, provide fundamental structural information regarding the encountered formation. Where the same fracture can be identified on both the images and the core, properly oriented borehole wall images also allow reorientation of cores, a key step in structural and paleomagnetic studies (MacLeod et al., 1995; Célerier et al., 1996; Goodall et al., 1998; Major et al., 1998; Haggas et al., 2001; Miller et al., 2003). Here, we investigate the validity of the orientation of FMS images in highly magnetized formations having potentially higher natural remanent magnetization (NRM $\geq$ 1 A/m) and/or magnetic susceptibility (MS $\geq 10^{-4}$ SI) than sedimentary formations (NRM $\leq 10^{-1}$ A/m; MS < 10^{-4} SI) for which the FMS was primarily developed.

Correction and orientation of FMS images are based on accelerometry and magnetometry measurements made with Schlumberger General-Purpose Inclinometry (GPI) modules such as the GPI Tool (GPIT) or the earlier GPI Capsule (GPIC) (see Robinson, Von Herzen, et al., 1989). The GPI modules use three-axis acceleration measurements to detect horizontal (shocks) and vertical (stick-slip and incomplete compensation of ship heave) movements. Three-axis magnetometers measure the intensities of the horizontal (Fx and Fy) and vertical (Fz) components of the local magnetic field (Fig. F1). From these components, intensity (F), declination (dec), and inclination (inc) of the total field in the tool frame are given by the following equations:

F1. Angular conventions and tool orientations, p. 14.

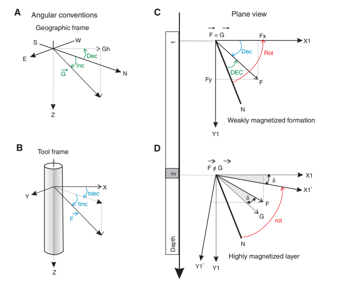

$$F = SQR(Fx^2 + Fy^2 + Fz^2),$$

$$dec = \arctan(Fy/Fx), \text{ and}$$

$$inc = \arctan(Fz/Fh),$$

where Fh = the horizontal component of the total magnetic field measured in the tool frame and is defined as

$$Fh = SQR(Fx^2 + Fy^2).$$

Actually, outputs of the Schlumberger GPIT are the raw Fx, Fy, and Fz components and the smoothed with depth total field (FNOR, filtered version of F), tool inclination (FINC, filtered version of inclination), and the tool azimuth (P1AZ, deduced from the comparison of the filtered version of declination with the locally tabulated declination at the site [DEC]) (see Table T1 for details on notation). This smoothing (filtering) operation is referred hereafter as the "Schlumberger algorithm."

T1. Notation, p. 22.

Thus, the GPI modules measure the properties of the local magnetic field, from which it is possible to deduce the orientation of the tool relative to north. When the field direction can be assumed to be constant, measured changes in the relative orientation of the field imply changes in tool rotation (Fig. F1). In particular, the rotation of the tool about its vertical axis can be measured relative to the component of the tabulated local geomagnetic field (Barton, 1997) in the plane perpendicular to the tool axis (Fig. F1C). In this case, the Schlumberger filtering operation is a data smoothing operation that reduces noise (high-frequency fluctuations). If the local magnetic field is not constant with depth but depends on the magnetic properties of the surrounding rocks, then this simple procedure may not work. In this case, the magnetometer's readings are not a simple linear function of the tool rotation but are a complex function integrating local magnetic direction variation with depth (Fig. F1D). In other words, the approximation that the total measured field is close to the international geomagnetic reference field (IGRF, see www.ngdc.noaa.gov/IAGA/vmod/igrf.html) is commonly valid for sedimentary formations but may break down and lead to incorrectly oriented FMS images for highly magnetized formations (e.g., oxide-rich layers) such as those drilled during ODP Legs 118, 176, and 197.

In connection with investigations of the physical and structural properties of formations containing alternating oxide-rich layers (Einaudi et al., in press), we present a methodological study checking, for the first time, the validity of the Schlumberger algorithm in such an environment. This algorithm was initially developed for sedimentary formations and is routinely used during ODP legs independent of formation type. First, based on data from subvertical ODP Hole 1203A (Leg 197), we investigate the frequency nature of the vertical and horizontal accelerations of the traditional ODP FMS-sonic logging tool string. These accelerations, respectively, reflect vertical and horizontal displacements of the tool. Based on the intrinsic low-frequency nature of the tool rotation, we propose to isolate the rotational component of the tool from the raw local magnetic field records using a low-frequency filtering algorithm. In order to prove the validity and efficiency of this simple filtering operation, we take advantage of the fact that an oriented borehole magnetometer, developed and designed by the Geophysical Institute of Göttingen, Germany (Göttingen Borehole Magnetometer, GBM) (Steveling et al., 1991), was deployed during Leg 197. This magnetometer is equipped with an optical gyro (Tarduno, Duncan, Scholl, et al., 2002) and provides direct and independent records of (1) the local total magnetic field and (2) the tool rotation by measuring its angular rotation rate with depth. Thus, with this data set, the tool orientation determined using a filtered version of the raw magnetic logs (magnetometer-based tool orientation) sensitive to potential magnetic anomalies can be compared with the true (optical-gyro based) tool orientation measured by the gyroscopic system. In the second step of our demonstration, we compare our previously validated algorithm with results obtained from the Schlumberger algorithm and validate the latter for highly magnetized (hard rock) environments. As additional proof of the validity of the latter algorithm for such formations, we finally compare the two discussed algorithms using data acquired from subvertical Hole 735B logged during Legs 118 and 176.

PHYSICAL BASIS OF NEW ALGORITHM

During logging operations and especially in oceanic environments such as those encountered during ODP legs, the logging tool string experiences more or less regular vertical (tool displacement, stick-slip, and heave) and horizontal (rotation and shock) movements. These movements are complex functions of the external conditions (hole shape, heave compensation, logging speed, cable length, etc.) and the tool itself (length, weight, and number of points of contact with the formation: centralizer and pads). In order to better assess the frequency spectrum of these movements, we inspected the normalized vertical and horizontal tool string accelerations recorded by the GPIT accelerometers in Hole 1203A (see "Downhole Measurements" in Shipboard Scientific Party, 2002). Analysis was performed using the continuous wavelet transform (WT), an alternative and generalization to the basic windowed Fourier transform for space-scale analysis.

Wavelet analysis (Morlet et al., 1982a, 1982b) provides an automatic localization of specific behaviors such as cyclic patterns or discontinuities, both in time and frequency (e.g., Daubechies, 1992; Torrence and Compo, 1998). In contrast to classical Fourier transform or windowed Fourier transform, which decomposes the original signal on the basis of an infinite periodic function depending on a unique parameter (frequency), the wavelet transform allows a "depth-scale" representation that depends on the (a) scale and (b) translation parameters. A reading of the wavelet power spectrum can be obtained by constructing a color diagram with the depth on the vertical axis, the scales on the horizontal axis and the modulus of the wavelet transform represented by patches of varying color (Torrence and Compo, 1998).

Applied to the normalized vertical and horizontal accelerations recorded at Site 1203 (Fig. F2A, F2C), this type of diagram reveals the frequency nature of ocean drilling tool string movements by deciphering the multiscale components of tool acceleration (Fig. F2B, F2D). The full normalized vertical acceleration record (191.0–916.2 meters below seafloor [mbsf]) is characterized by (1) a high-frequency component (<5 m) associated with heave and (2) localized stick-slip displacement over intervals of small (<20 m) and intermediate (~40–60 m) scale. Whereas the high-frequency component could be explained by incomplete heave compensation, the other components are directly linked to hole conditions, in particular hole shape (Fig. F2E). In contrast, the horizontal record (Fig. F2D) is very simple and is characterized by a component of distinct low frequency within the ~40–160 m range. A comparison of the wavelet representations of the horizontal acceleration with hole shape shows that the intervals where tool acceleration changes are limited by the tool string length (~40 m) and correspond to changes in hole diameter (Fig. F2E). Whereas vertical movements are often "jerky," the horizontal component of the tool is smooth and characterized by a low-frequency content with a wavelength about one-half the tool string length.

F2. Wavelet analysis of FMS-sonic tool string, p. 15.

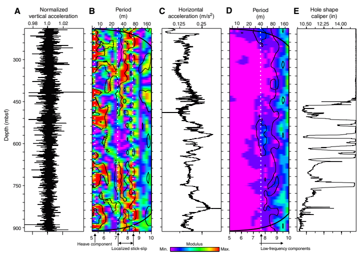

Using raw magnetic records, tool string orientation (rot) in the borehole is indirectly estimated by comparing the declination measured in the tool frame (tdec) (i.e., angle between the horizontal component of the total field and the tool housing reference line [x-axis]) and the tabulated declination of the geomagnetic field (DEC) (Fig. F1) (Barton, 1997). Whereas the discrepancy between the measured local field and the tabulated field at seafloor never exceeds ±5°, rapid changes in magnetic properties with depth can locally add anomalous field components that can in turn perturb the estimated value of the tool rotation (Fig. F1D). In that case, the horizontal component of the local total magnetic field (Fx and Fy) logs integrates (1) a low-frequency rotational component, as has been demonstrated above, and, possibly, (2) a high-frequency perturbed "declination" component associated with highly magnetized/permeable materials such as oxide-rich layers. Because of the frequency difference between these two components, a simple frequency filtering algorithm was developed to isolate the rotational component necessary to properly orient the FMS images from the indirect raw magnetic records of the GPI modules.

DATA AND VALIDATION OF NEW ALGORITHM

Hole 1203A

Leg 197 was devoted to studying the motion of the Hawaiian hotspot from a paleomagnetic point of view (Tarduno, Duncan, Scholl, et al., 2002). Two tools were used to log magnetic data in Hole 1203A (see "Downhole Measurements" in Shipboard Scientific Party, 2002), the GPIT in combination with the classic FMS-sonic tool string (~40 m long) and the oriented GBM (Tarduno, Duncan, Scholl, et al., 2002).

The GBM was originally used to monitor magnetic field variations in a borehole continuously for several weeks and to compare these with field variations at depth (Steveling et al., 1991). The GBM tool consists of three fluxgate sensors that log the horizontal (Fx and Fy) and vertical (Fz) components of the magnetic flux density. The tool is equipped with an angular rate sensor (LITEF) to monitor the spin history around the z-axis and variations around the x- and y-axes during a logging run. The LITEF miniature fiber-optic rate sensor provides angular rate output. The rate sensor is an unconventional gyroscope, since it does not have a spinning wheel. It detects and measures angular rates by measuring the frequency difference between two counter-rotating light beams. When the gyro is at rest, the two beams have identical frequencies. When the gyro is subjected to an angular turning rate around an axis perpendicular to the plane of the two beams, one beam then has a greater optical path length than the other. Therefore, the two resonant frequencies change and the resulting differential frequency measured by optical means provides a direct digital output of the rotational component. This oriented magnetometer has an advantage over conventional (nonoriented) magnetometers because it is independent of the magnetic properties of the formation. We will use that property to test the effects of NRM and MS on the determination of the rotation of the tool string using nonoriented magnetometers.

Based on logging data, the penetrated formation at Site 1203 is composed of volcaniclastic sediments alternating with volcanic rocks (Fig. F3A). Rock magnetic measurements on sediments and basalts give MS values from 10^{-4} to 10^{-2} SI and 10^{-3} to 10^{-1} SI, respectively, and NRM values from 10^{-3} to 10^{-1} A/m and 1 to 10 A/m, respectively (Shipboard Scientific Party, 2002). The use of the GBM and the alternating sediments and basalts at this site provide a unique opportunity to test the proposed algorithm by comparing the tool string rotation obtained from filtering the magnetic tool declination record with the rotation deduced from the gyroscopic system.

The magnetic records from the GBM within the open hole (464–916 mbsf) correspond very well to those from the GPIT (Tarduno, Duncan, Scholl, et al., 2002) (Fig. F4A, F4B). Within sedimentary sections, the mean total field, F, is close to the expected 48,800 nT and the magnetic inclination derived from magnetic logging is ~63°, close to the expected 62° for this latitude according to IGRF2000 (Geomag version 4.0, available online at **www.ngdc.noaa.gov/seg/geom_util/geomutil.shtml**) (Fig. F3B, F3C). In the underlying basement sedimentary alternating sections, high and localized variations in the magnetic field are encountered that correlate well with lithology. Highly magnetized layers correlate with sequences of massive basalts and pillows and are interrupted by intervals of volcaniclastic sediments (Shipboard Scientific Party, 2002). The direct declination (Dec), the GBM tool declination (tdec) deduced from the raw magnetic records (Fx, Fy, and Fz), and the direct (optical-gyro based) rotation (Rot) are presented in Figure F3D, F3E, and F3G, respectively. Notations are summarized in Table T1. The mean declination is slightly and uniformly higher than the expected –1.5°, possibly due to a calibration or tool housing problem. The low-frequency trend (increase) in declination in the lower 40 m of the open hole is discussed in **"Discussion and Conclusions,"** p. 9. In general, the GBM rotated smoothly and at low wavelength during the run (mean rate of rotation = 1 rotation/~40 m), confirming our basic hypothesis on the frequency nature of rotation of downhole logging tools (Fig. F3G). As exemplified by the correlation (especially in the 550- to 750-mbsf depth interval) between the hole shape (Fig. F3F) and Rot (Fig. F3G), orientation of the tool is mainly guided by hole shape (Fig. F3F), which is strongly associated with lithology changes (Fig. F3A). An additional high-frequency component of weak amplitude due to (1) the small size and lack of a contact point between the tool and the borehole, (2) tool and cable friction on the borehole wall, as well as (3) ver-

F3. GBM magnetic and orientation logs, p. 16.

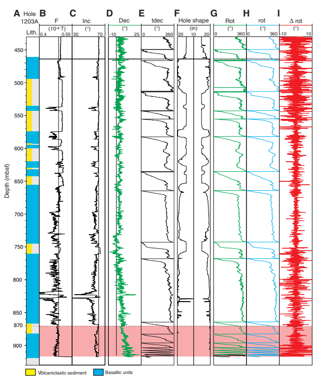

F4. GBM and GPIT magnetic logs, p. 17.

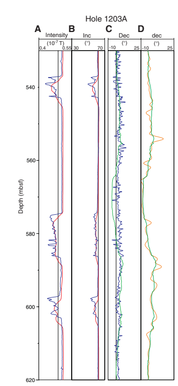

tical tool displacement (stick-slip and heave) is also present in the optical-gyro-based record of Rot (Fig. F3G).

ALGORITHM VALIDATION USING THE GBM DIRECT ROTATION RECORD

To validate the algorithm we developed, we determine the GBM rotational component (rot) indirectly (Fig. F3H) by filtering the equivalent raw magnetic records (tdec obtained from Fx, Fy, and Fz) as it was obtained by a GPI module (Fig. F3H) and compare our results with the direct GBM rotation data (Rot) (Fig. F3G).

Various low-filtered versions of the data can be obtained by convolving various type and width of filters with the original data. The boxcar, cosine arch, and Gaussian filters are all linear operators, and their effect on the frequency content of the data (the transfer function) can be calculated (Fig. F5). The boxcar filter is a simple running average, whereas the cosine, Gaussian, and Hamming filters are weighted running averages. In the following, we tested these four types of filters for width ranging from 2 m (approximate heave) to 20 m (about one-half of the tool string length). As an example, the residual (Δrot) between the filtered component using a cosine filter of 4 m width (rot; Fig. F3H) and Rot (Fig. F3G) is shown in Figure F3I. This comparison shows a good match (residuals mostly <10°) between the indirect (magnetometer based) and direct (optical-gyro based) records and thus validates our filtering algorithm. Quality of the filtering algorithm can also be estimated by comparing the resulting declination with that measured by the GBM (Fig. F4C). The difference between the two records is mostly within 10° and does not impair the computation of the tool orientation. Similar results were found with other combinations of types and widths of filters.

F5. Filters used in this study, p. 18.

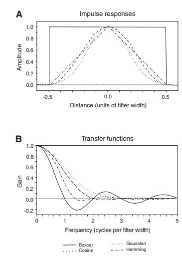

COMPARISON OF THE VALIDATED ALGORITHM WITH THE STANDARD SCHLUMBERGER ALGORITHM: VALIDATION OF THE SCHLUMBERGER ALGORITHM

Hole 1203A

The application of the previously validated algorithm to the magnetic records from the GPIT on the FMS-sonic tool string allows us to compare our filtering algorithm with the standard algorithm (here referred to as the Schlumberger algorithm) routinely used to compute tool orientation during ODP legs. Magnetic logs of FMS-sonic tool string passes 1 and 2 are of excellent quality, as attested by the repeatability of the intensity and inclination of the local total field (Figs. F4A, F4B, F6A, F6B). Figure F6C shows the tool declination (tdec) of FMS-sonic passes 1 and 2, integrating total field declination (Dec) and the rotational component (Rot). From the bridge located at ~560 mbsf, guided by hole shape (Fig. F6D) and cable properties, both passes use the same path, thus restricting the study to the first pass. Figure F6E–F6H compares the tool string rotational components isolated using our proposed algorithm (cosine filter of 4 m width and boxcar filter of 10 m width) and that of the Schlumberger algorithm. As attested by the resid-

F6. FMS-sonic magnetic logs, p. 19.

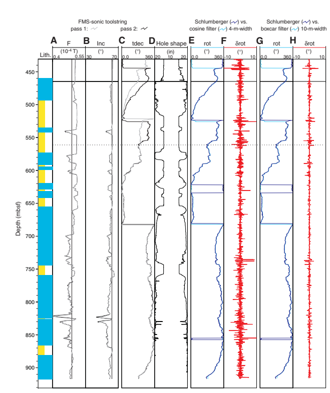

ual (δrot) between these two components (Fig. F6F, F6H), results are in good accordance (mostly within 5°) and validate the use of the Schlumberger algorithm in such an environment. A comparison of the declination obtained at this site using both algorithms is given in Figure F4D.

The two-step demonstration above shows that independent of the geometric parameters of the tool string (length, diameter, and number of points of contact), the proposed algorithm can be validated by comparing the GBM direct (optical-gyro based) rotation record with a filtered version of its bulk magnetic parameters. This well-documented algorithm was next compared with the standard Schlumberger algorithm, initially developed for weakly magnetized (sedimentary) formations. The good agreement between results validates the use of the latter in magnetically contrasted and layered formations. As an additional test for the validity of these algorithms, we applied both to magnetic records from reference Hole 735B, which were acquired using other tool string configurations.

Hole 735B

Hole 735B was logged during ODP Legs 118 and 176, providing a common logged section of more than 500 m. During Leg 118, downhole magnetic measurements were performed with the same U.S. Geological Survey (USGS) susceptibility probe used during ODP Leg 102 (Bosum and Scott, 1988) and the nonoriented magnetometer in the Schlumberger GPIC run in conjunction with the Schlumberger Lithodensity Tool (LDT). During ODP Leg 176, magnetic data were recorded by the Schlumberger GPIT, first run in conjunction with the Dual Resistivity Lateral Log (DLL) tool string and then with the FMS-sonic tool string. Because digital records of the USGS magnetometer are not available, direct validation as in the previous data set is impossible. However, the set of magnetic logs recorded by the GPI modules gives us the opportunity to compare the standard Schlumberger algorithm used at this time with the filtering algorithm previously validated.

The lithostratigraphy of Site 735 (50–600 mbsf) is presented in detail in Dick et al. (1991) for the Leg 118 cores and Dick, Natland, Miller, et al. (1999) for the Leg 176 cores. Gabbroic rocks constitute >99 vol% of the total section. This section is composed of five principal gabbroic units and more secondary intrusive units, a number of them late small ferro-gabbro intrusions (Fig. F7A). The igneous stratigraphy is primarily controlled by the interconnection between deformation, magma segregation, and crystallization (Dick, Natland, Miller, et al., 1999). Shipboard laboratory measurements on minicores from Hole 735B (core recovery = 86.6%) indicated that the gabbroic rocks have a mean MS of 23×10^{-3} SI (maximal value ~ 10^{-1} SI) and a mean NRM of 2.5 A/m (26×10^{-5} to 130 A/m). In accordance with core measurements (Fig. F7B, dots), the MS log (Fig. F7B, continuous line) made with the USGS susceptibility tool (30–490 mbsf) indicates that the MS of gabbro in the upper 215-m section of the hole is extremely variable, with one thin zone approaching 0.5×10^{-3} SI and many thin anomalies peaking out between 10×10^{-3} and 25×10^{-3} SI, but with many other values approaching zero. Midway downhole (centered at ~245 mbsf), a 60-m zone of high MS (~30×10^{-3} to 55×10^{-3} SI) occurs in a gabbroic section containing anomalously high concentrations of magnetite and ilmenite. Below the magnetite-ilmenite-rich gabbros, a 100-m-thick magnetically quiet zone occurs, with MS averaging 1×10^{-3} to 10×10^{-3} SI. Below this

F7. Hole 735B magnetic logs, p. 20.

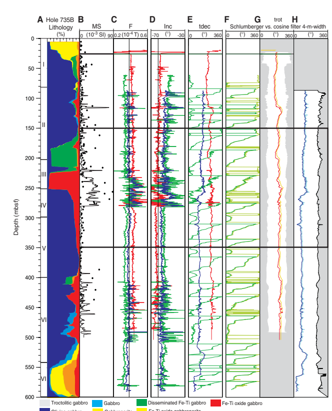

zone, another highly variable 100-m-thick interval occurs near the bottom of the hole, with MS in the range of 5×10^{-3} to 40×10^{-3} SI (Pariso et al., 1991; Kikawa and Pariso, 1991). This interval is also characterized by high magnetite and ilmenite concentration in the drill cores.

Figure **F7C** shows that the intensities of the total magnetic field for both the GPIC (Leg 118, in red) and the GPIT (Leg 176, FMS in blue and DLL in green) have the same shape and relative amplitudes but are offset by a constant. The shift between the two tool generations could have resulted from calibration problems and/or imperfect magnetic isolation of the GPIC. Although in sedimentary sections, total magnetic intensity and inclination are close to the expected values at this latitude (38,348 nT and –61.5°, respectively), two significant increases in the intensities as well as changes in the inclination logs can be observed in oxide-rich sections (Fig. **F7C, F7D**): the first between 220 and 285 mbsf and the second between 410 and 510 mbsf.

Figure **F7E** presents the tool declination (tdec) log, which contains both the rotational component and declination of the local magnetic field, as recorded by the three tool strings. For these tool strings, isolated tool rotation (rot) deduced by our filtering operation is compared with that deduced from the Schlumberger algorithm (Fig. **F7F–F7H**). For the two algorithms and independent of the lithology, the short and no-contact-point DLL tool string continuously rotated (mean rate of rotation = 1 rotation/~25 m) over the whole section (~60–580 mbsf). On the contrary, because of friction between the tool string and borehole walls, the long and one-contact-point (centralizer) LDT tool string as well as the long and multiple-contact-points (four pads and centralizer) FMS-sonic tool string did not rotate significantly during the logging operation. This small rate of rotation may also be indicative of hole ellipticity, deviation, or directional borehole damage caused by the extensive fishing operations following the break-off of drill pipe in the hole. Independent of the tool string geometry, residuals (δrot) between the developed algorithm and the Schlumberger algorithm are <6° (not shown), thus confirming the use of the Schlumberger algorithm in such formations. On the other hand, observed tool rotations at this site confirm the initial finding that tool rotation is intrinsically of higher wavelength (approximately tool string length) than the local fluctuations of the magnetic field (meter scale). In such cases, filtering techniques using filters between 2 and 10 m length lead to correctly oriented borehole wall images.

DISCUSSION AND CONCLUSIONS

FMS microresistivity images of borehole walls provide valuable information in exploring the structure and history of oceanic crust. However, the use of these images for structural or core orientation purposes relies on the accuracy of image orientation. In a two-step demonstration involving complementary data sets and a newly developed algorithm, we validated the use of the Schlumberger algorithm, routinely used during ODP cruises, for highly magnetized (hard rock) formations. The basic hypotheses of the two algorithms discussed in this paper are as follows: (1) the dynamics (rotation) of the tool string are intrinsically smooth (of low frequency/wavelength) and (2) the local field fluctuations associated with the oxide-rich layers (thin enough and separated by distance large enough to produce only high-frequency fluctuations in the magnetic records) locally add up a high-frequency component that can be removed by simple filtering operations. Space-scale analysis based on continuous wavelets demonstrated the low-frequency behavior of the tool string rotation in a subvertical borehole. However, at each site, the high-frequency nature of the local anomalous field still needs to be proven. Depending on the geometry (thickness and separating distance), as well as contrasts in magnetic properties (NRM and MS) of the penetrated formations, the local anomalous magnetic field may integrate additional intermediate and low-frequency components along with the referenced geomagnetic field (Parker and Daniell, 1979; Ponomarev and Nechoroshkov, 1983, 1984). An example of such configuration (low-frequency trend) may be visible in the lower portion (870–920 mbsf) of ODP Hole 1203A (Fig. **F3D**). A similar local low-frequency trend can be expected, for example, at basement contacts where a poorly and uniformly magnetized sedimentary formation is deposited over a thick and highly magnetized basement (Ponomarev and Nechoroshkov, 1983). Using the equations given by Pozzi et al. (1988), computation of the magnetic field in the borehole given the known remanent magnetization (or known induced magnetization) of the formation may help to quantify the effect of the magnetization on the determination of the tool orientation in terms of intensity and wavelength. For example, at Site 735, a magnetization of 1 A/m produces a field of 1,145 nT in the borehole (compared to the main field of 38,400 nT at the site). On the other hand, in addition to the high-frequency effects of oxide-rich layers, other sources such as pipes, casings, basement, and/or magnetic storms can perturb the geomagnetic field in a large spectrum of frequencies, and Bosum and Scott (1988) urge caution, as the proposed filtering techniques will fail.

At present, for ongoing ODP exploration, there are no technical development plans to replace the indirect orientation module (GPIT) of the FMS and UBI tool strings with direct-orientation gyroscopic systems. Hence, in light of both the actual ODP legs and in consideration of (1) the objectives of the future Integrated Ocean Drilling Program (IODP) expeditions, (2) the magnetic properties of penetrated formations, (3) available technical means, as well as (4) time constraints, the following methods are recommended to check tool orientation.

For accurate FMS-based structural investigations or core orientation within highly magnetized formations, a direct and independent log of the total magnetic declination is highly recommended. This log can only be obtained by running an oriented magnetometer associated with a gyroscopic system. Then, this direct record of declination can be compared with the magnetic parameters of the GPIT of the actual FMS-sonic or UBI tool strings. Provided that the magnetometers have similar sensitivity and are logged at similar speeds, one can back-orient the FMS-sonic or UBI tool string using oriented magnetometer logs and double-check the tool rotation computed by filtering techniques.

F8. Estimation of filtering quality, Hole 735B, p. 21.

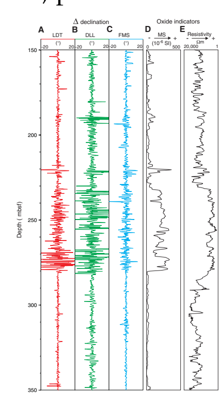

If, because of lack of time or availability, oriented magnetometers cannot be run, data processing/analysis is necessary. Depending on the frequency nature (high, intermediate, and/or low) of the magnetic anomalies and tool rotation, simple or more sophisticated (nonlinear/adaptative) filtering techniques and complementary analyses must be involved. An example of complementary analysis (quality check) where we take advantage of the use of GPIT logs in combination with different tools is described in Figure **F8.** In this example we compare the indirect declinations (Δdec)—local properties of the formation—deduced from various tool strings with (1) lithological information as well as (2) oxide indicators such as NRM, MS, and/or resistivity logs. Correlation between these logs allows a raw estimation of tool string orientation quality, but in any case does not replace the direct record that oriented magnetometers can provide.

Development of nonlinear/adaptative techniques is in progress. The developed algorithm is based on the multiscale analysis of available magnetic logs. Multiscale analysis using the continuous wavelet transform helps to decipher the multiscale components of magnetic anomalies and tool rotation behavior. However, until we can complete this analysis with geological constraints (lithology), doubts on the estimation of the tool rotation may exist as a consequence of a poorly constrained inversion scheme capable of isolating the rotation component from raw magnetic logs. For now, this detailed study on natural cases encountered during ODP legs is a first step in providing guidelines and error limits for less documented past or future holes.

ACKNOWLEDGMENTS

We thank Drs. A. Etchecopar and P. Cheung from the Schlumberger-Riboud Product Center (France) for their pre-review of the manuscript and their general comments on the manuscript and the filtering techniques used. We also thank S. Primm and B. Tikoff (Department of Geology, University of Wisconsin, USA) for improvements to the English, as well as Gary Acton (Department of Geology, University of California, Davis, USA), Trevor Williams (Borehole Research Group, Lamont-Doherty Earth Observatory, University of Columbia, USA), and Lorri Peters (IODP, Texas A&M University, USA) for their careful review of the manuscript. This research used data provided by the Ocean Drilling Program (ODP). ODP is sponsored by the U.S. National Science Foundation (NSF) and participating countries under management of Joint Oceanographic Institutions (JOI), Inc. Figures were drawn using the Generic Mapping Tools package developed by Wessel and Smith (1995).

REFERENCES

Ayadi, M., Pezard, P.A., Laverne, C., and Bronner, G., 1998. Multi-scalar structure at DSDP/ODP Site 504, Costa Rica Rift, I: stratigraphy of eruptive products and accretion processes. *In* Harvey, P.K., and Lovell, M.A. (Eds.), *Core-Log Integration.* Geol. Soc. Spec. Publ., 136:297–310.

Barton, C.E., 1997. International geomagnetic reference field: the seventh generation. *J. Geomagn. Geoelectr.,* 49:123–148.

Bosum, W., and Scott, J.H., 1988. Interpretation of magnetic logs in basalt, Hole 418A. *In* Salisbury, M.H., Scott, J.H., et al., *Proc. ODP, Sci. Results,* 102: College Station, TX (Ocean Drilling Program), 77–95.

Brewer, T.S., Harvey, P.K., Lovell, M.A., Haggas, S., Pezard, P.A., and Goldberg, D., 1999. Borehole images of the ocean crust: case histories from the Ocean Drilling Program. *In* Lovell, M.A., Williamson, G.M., and Harvey, P.K. (Eds.), *Borehole Images: Application and Case Histories*. Geol. Soc. Spec. Publ., 159:283–294.

Brewer, T.S., Harvey, P.K., Lovell, M.A., Haggas, S., Williamson, G., and Pezard, P., 1998. Ocean floor volcanism: constraints from the integration of core and downhole logging measurements. *In* Harvey, P.K., and Lovell, M.A. (Eds.), *Core-Log Integration*. Geol. Soc. Spec. Publ., 136:341–362.

Célérier, B., MacLeod, C.J., and Harvey, P.K., 1996. Constraints on the geometry and fracturing of Hole 894G, Hess Deep, from Formation MicroScanner logging data. *In* Mével, C., Gillis, K.M., Allan, J.F., and Meyer, P.S. (Eds.), *Proc. ODP, Sci. Results,* 147: College Station, TX (Ocean Drilling Program), 329–345.

Daubechies, I., 1992. *Ten Lectures on Wavelets:* Philadelphia (Soc. Ind. Appl. Math.).

Dick, H.J.B., Meyer, P.S., Bloomer, S., Kirby, S., Stakes, D., and Mawer, C., 1991. Lithostratigraphic evolution of an in-situ section of oceanic Layer 3. *In* Von Herzen, R.P., Robinson, P.T., et al., *Proc. ODP, Sci. Results,* 118: College Station, TX (Ocean Drilling Program), 439–538.

Dick, H.J.B., Natland, J.H., Miller, D.J., et al., 1999. *Proc. ODP, Init. Repts.,* 176: College Station, TX (Ocean Drilling Program).

Einaudi, F., Pezard, P., Ildefonse, B., and Glover, P., in press. Electrical properties of gabbros from Hole 1105A, Southwest Indian Ridge. *J. Geol. Soc. (London, U.K.).*

Goldberg, D., 1997. The role of downhole measurements in marine geology and geophysics. *Rev. Geophys.,* 35:315–342.

Goodall, T.M., Møller, N.K., and Rønningsland, T.M., 1998. The integration of electrical image logs with core data for improved sedimentological interpretation. *In* Harvey, P.K., and Lovell, M.A. (Eds.), *Core-Log Integration.* Geol. Soc. Spec. Publ., 136:237–248.

Kikawa, E., and Pariso, J.E., 1991. Magnetic properties of gabbros from Hole 735B, Southwest Indian Ridge. *In* Von Herzen, R.P., Robinson, P.T., et al., *Proc. ODP, Sci. Results,* 118: College Station, TX (Ocean Drilling Program), 285–307.

Haggas, S., Brewer, T.S., Harvey, P.K., and Iturrino, G., 2001. Relocating and orienting cores by the integration of electrical and optical images: a case study from Ocean Drilling Program Hole 735B. *J. Geol. Soc. (London, U.K.),* 158:615–623.

Lovell, M.A., Harvey, P.K., Brewer, T.S., Williams, C., Jackson, P.D., and Williamson, G., 1998. Application of FMS images in the Ocean Drilling Program: an overview. *In* Cramp, A., MacLeod, C.J., Lee, S.V., and Jones, E.J.W. (Eds.), *Geological Evolution of Ocean Basins: Results from the Ocean Drilling Program.* Geol. Soc. Spec. Publ., 131:287–303.

MacLeod, C.J., Célérier, B., and Harvey, P.K., 1995. Further techniques for core reorientation by core-log integration: application to structural studies of lower oceanic crust in Hess Deep, eastern Pacific. *Sci. Drill.,* 5:77–86.

Major, C.O., Pirmez, C., Goldberg, D., and the Leg 166 Scientific Party, 1998. High-resolution core-log integration techniques: examples from Ocean Drilling Program. *In* Harvey, P.K., and Lovell, M.A. (Eds.), *Core-Log Integration*. Geol. Soc. Spec. Publ., 136:285–295.

Miller, D.J., Iturrino, G.J., and McGuire, J.C., 2003. Core-log correlations in oceanic basement from Hole 1105A on the Southwest Indian Ridge. *In* Casey, J.F., and Miller, D.J. (Eds.), *Proc. ODP, Sci. Results,* 179 [Online]. Available from World Wide Web: <http://www-odp.tamu.edu/publications/179_SR/chap_03/chap_03.htm>. [Cited 2004-08-30]

Morlet, J., Arens, G., Fourgeau, E., and Giard, D., 1982a. Wave propagation and sampling theory, 1. Complex signal and scattering in multilayered media. *Geophysics,* 47:203–221.

Morlet, J., Arens, G., Fourgeau, E., and Giard, D., 1982b. Wave propagation and sampling theory, 2. Sampling theory and complex waves. *Geophysics,* 47:222–236.

Pariso, J.E., Scott, J.H., Kikawa, E., and Johnson, H.P., 1991. A magnetic logging study of Hole 735B gabbros at the Southwest Indian Ridge. *In* Von Herzen, R.P., Robinson, P.T., et al., *Proc. ODP, Sci. Results,* 118: College Station, TX (Ocean Drilling Program), 309–321.

Parker, R.L., and Daniell, G.J., 1979. Interpretation of borehole magnetometer data. *J. Geophys. Res.,* 10:5467–5479.

Pezard, P.A., and Luthi, S.M., 1988. Borehole electrical images in the basement of the Cajon Pass scientific drillhole, California: fracture identification and tectonic implications. *Geophys. Res. Lett.,* 15:1017–1020.

Pezard, P.A., Anderson, R.N., Howard, J.J., and Luthi, S.M., 1988. Fracture distribution and basement structure from measurements of electrical resistivity in the Cajon Pass scientific drillhole, California. *Geophys. Res. Lett.,* 15:1021–1025.

Ponomarev, V.N., and Nechoroshkov, V.L., 1983. First measurements of the magnetic field within the ocean crust: Deep Sea Drilling Project Legs 68 and 69. *In* Cann, J.R., Langseth, M.G., Honnorez, J., Von Herzen, R.P., White, S.M., et al., *Init. Repts. DSDP,* 69: Washington (U.S. Govt. Printing Office), 271–279.

Ponomarev, V.N., and Nechoroshkov, V.L., 1984. Downhole magnetic measurements in oceanic crustal Hole 395A on the Mid-Atlantic Ridge. *In* Hyndman, R.D., Salisbury, M.H., et al., *Init. Repts. DSDP,* 78 (Pt. B): Washington (U.S. Govt. Printing Office), 731–739.

Pozzi, J.-P., Martin, J.P., Pocachard, J., Feinberg, H., and Galdeano, A., 1988. In situ magnetostratigraphy: interpretation of magnetic logging in sediments. *Earth Planet. Sci. Lett.,* 88:357–373.

Rider, M.H., 1996. *The Geological Interpretation of Well Logs* (2nd ed.): Caithness (Whittles Publishing).

Robinson, P.T., Von Herzen, R., et al., 1989. *Proc. ODP, Init. Repts.,* 118: College Station, TX (Ocean Drilling Program).

Serra, O., 1989. *Formation MicroScanner Image Interpretation:* Houston (Schlumberger Educ. Services), SMP-7028.

Shipboard Scientific Party, 2002. Site 1203. *In* Tarduno, J.A., Duncan, R.A., Scholl, D.W., et al., *Proc. ODP, Init. Repts.,* 197 [Online]. Available from World Wide Web: http://www-odp.tamu.edu/publications/197_IR/chap_03/chap_03.htm. [Cited 2004-08-30]

Steveling, E., Spitzer, K., and Leven, M., 1991. Vertical gradient of horizontal geomagnetic variations—first results with the new Goettingen Borehole Magnetometer in the KTB-VB pilot hole. *Sci. Drill.,* 2:180–187.

Tarduno, J.A., Duncan, R.A., Scholl, D.W., et al., 2002. *Proc. ODP, Init. Repts.,* 197 [Online]. Available from World Wide Web: http://www-odp.tamu.edu/publications/197_IR/197ir.htm. [Cited 2004-08-30]

Torrence, C., and Compo, G.P., 1998. A practical guide to wavelet analysis. *Bull. Am. Meteorol. Soc.,* 79:61–78.

Wessel, P., and Smith, W.H.F., 1995. New version of the Generic Mapping Tools released. *Eos, Trans. Am. Geophys. Union,* 76:329.

Wilson, D.S., Teagle, D.A.H., Acton, G.D., et al., 2003. *Proc. ODP, Init. Repts.,* 206 [Online]. Available from World Wide Web: <http://www-odp.tamu.edu/publications/206_IR/206ir.htm>. [Cited 2004-08-30]

Figure F1. Angular conventions and tool orientation determination. **A.** In the geographic frame the geomagnetic field vector ($\vec{G}$) is described in terms of intensity (G), magnetic declination (Dec = angle formed between true north [N] and the projection of $\vec{G}$ on the horizontal plane), and magnetic inclination (Inc, also called magnetic dip = angle measured from the horizontal plane positively down to the magnetic field vector). **B.** In the tool frame, the local total magnetic field ($\vec{F}$) is described in terms of intensity (F), declination (tdec), and inclination (tinc). **C.** In plane view, estimation of the tool orientation, related to the instantaneous rotation of the tool with respect to N, is made by comparing the declination (Dec) of the local magnetic field to the tabulated declination (DEC) of the geomagnetic field (see Table T1, p. 22, for details on notation). **D.** When highly magnetized layers are present in the formation, the measured declination of the total magnetic field $\vec{F}$ is different from the theoretical value of the geomagnetic field ($\vec{G}$) by an angle (δ) leading to an equal bias in the local estimation of tool rotation. X1 = real orientation of the tool x-axis, X1′ = apparent orientation of the tool.

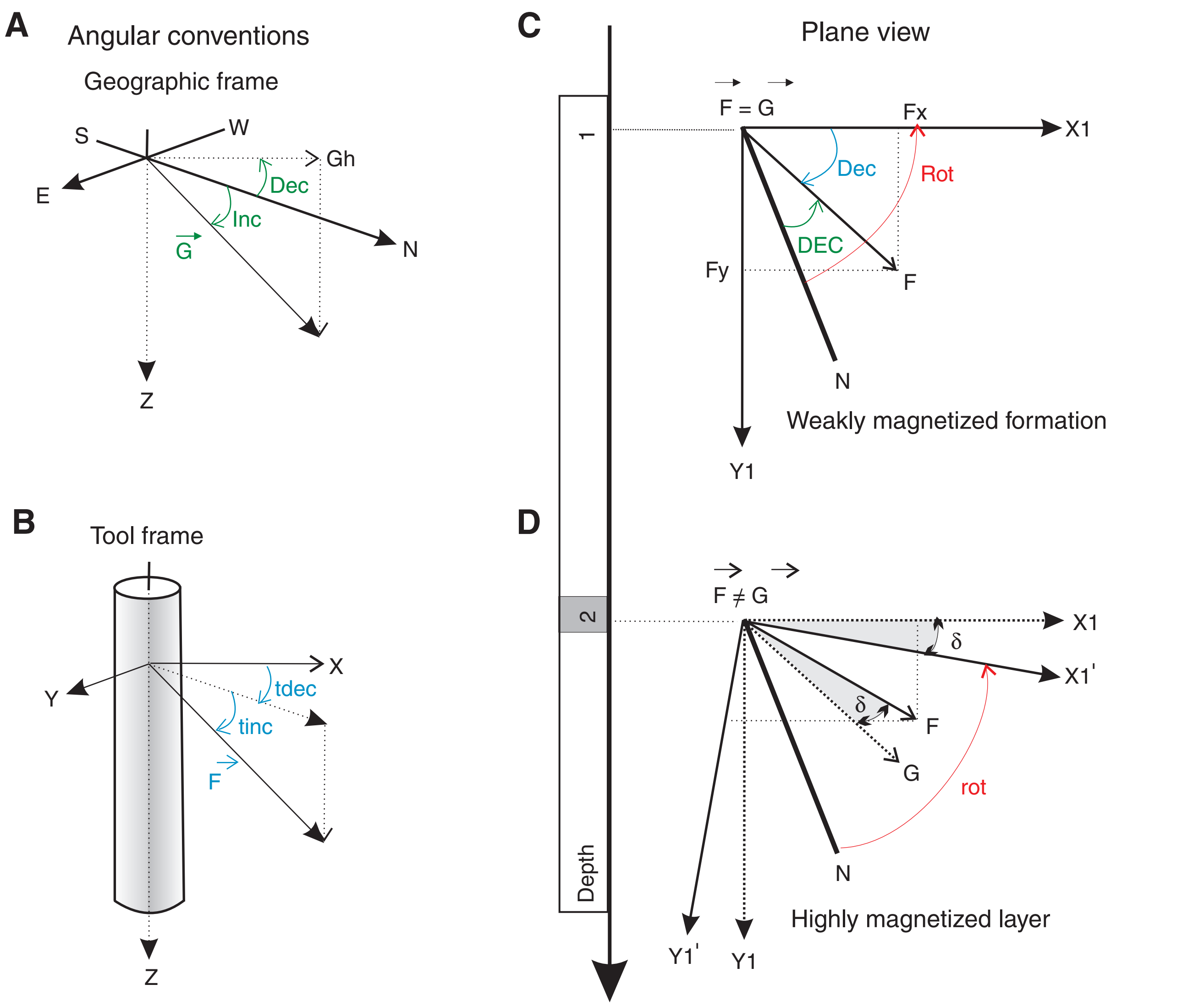

Figure F2. Wavelet analysis of the normalized vertical and horizontal acceleration of the Formation MicroScanner (FMS)-sonic tool string in Hole 1203A. **A.** Normalized vertical acceleration. **B.** Wavelet spectrum (modulus) of the normalized vertical acceleration showing incomplete heave compensation (~2 m) over the full record and localized stick-slip displacement over intervals of small (<20 m) and intermediate (~40–60 m) scale. **C.** Horizontal acceleration. **D.** Wavelet spectrum (modulus) of the horizontal acceleration showing a component of distinct low frequency within the 40- to 160-m range. **E.** Associated with D, hole shape expressed by the FMS tool string calipers. Hole shape exemplifies the effects of hole conditions on the tool rotation. Red = high wavelet modulus, blue = low wavelet modulus.

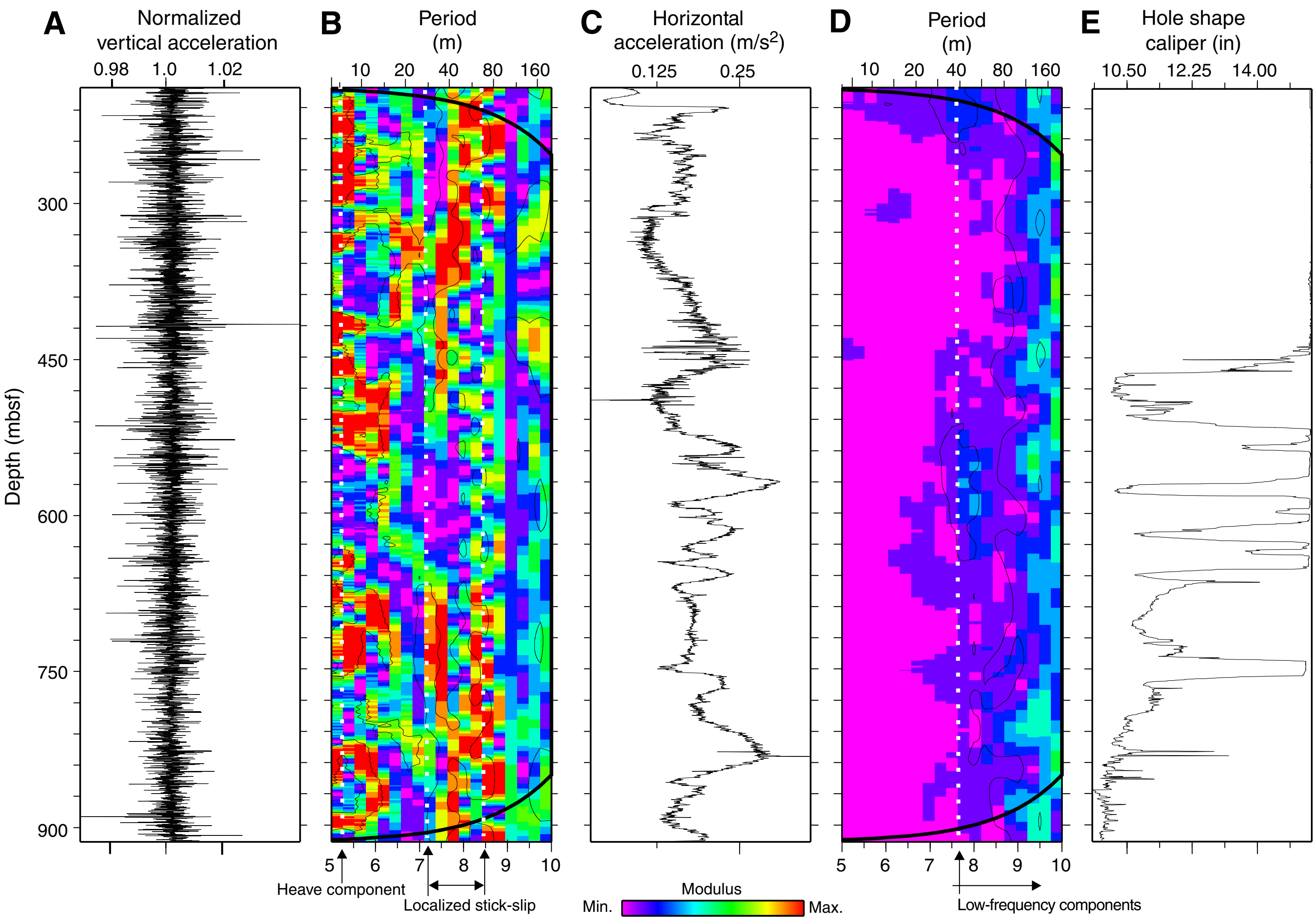

Figure F3. Hole 1203A magnetic and orientation logs from the orientated Göttingen Borehole Magnetometer (GBM) and comparison of the direct (optical-gyro based) estimation of the tool rotation with the proposed filtering algorithm. **A.** Lithology. **B.** Intensity of the total magnetic field (F). **C.** Inclination (Inc). **D.** Declination (Dec). **E.** Tool declination (tdec) obtained from raw magnetic records Fx, Fy, and Fz, integrating the local value of the declination and the tool rotation component (tdec = Dec + Rot). **F.** Hole shape. **G.** Rotation (Rot) directly recorded by the GBM gyroscopic system. **H.** Indirect GBM rotation (rot) obtained by filtering tdec using a 4-m-wide cosine filter. **I.** Residual (Δrot) between Rot and rot.

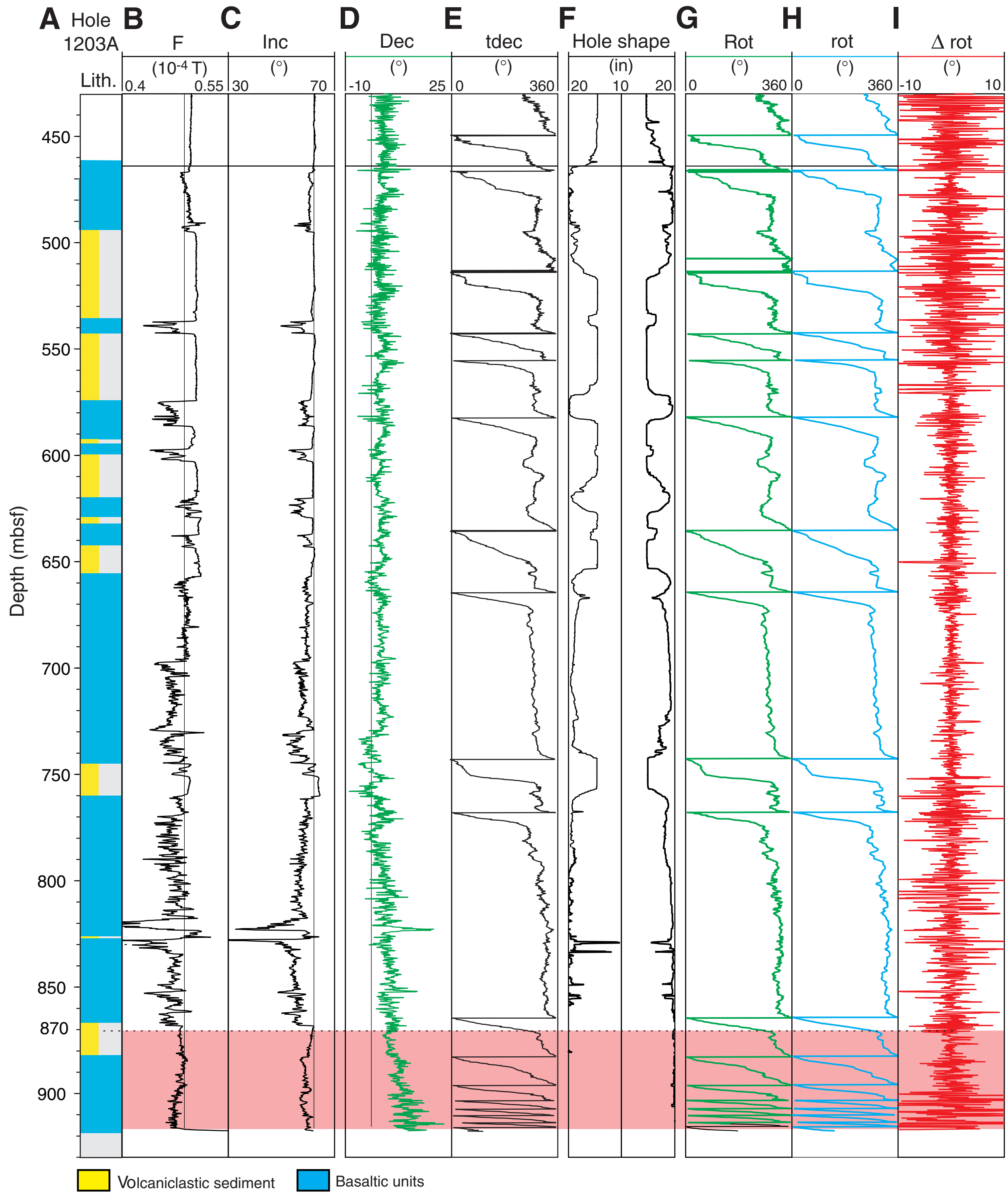

Figure F4. Hole 1203A magnetic logs from the orientated Göttingen Borehole Magnetometer (GBM) and Schlumberger's General Purpose Inclinometry Tool (GPIT). (**A**) Intensity (F) and (**B**) inclination (Inc) by GBM (blue) and FMS-sonic GPIT (red). Note the good match at the meter scale between these logs. **C.** Comparison between the direct GBM declination (Dec) (blue) and deduced declination (dec) using the proposed algorithm (4-m-wide cosine filter, light green) from GBM raw magnetic logs (Fx, Fy, and Fz). Due to the filtering operating, high-frequency fluctuations (<10°) in the declination are smoothed without affecting the indirect computation of the GBM rotation from its raw magnetic parameters. **D.** Comparison of the declination records deduced from the GPIT raw magnetic logs using our algorithm (4-m-wide cosine filter, dark green) and the Schlumberger algorithm (2.4-m-wide Hamming filter, orange).

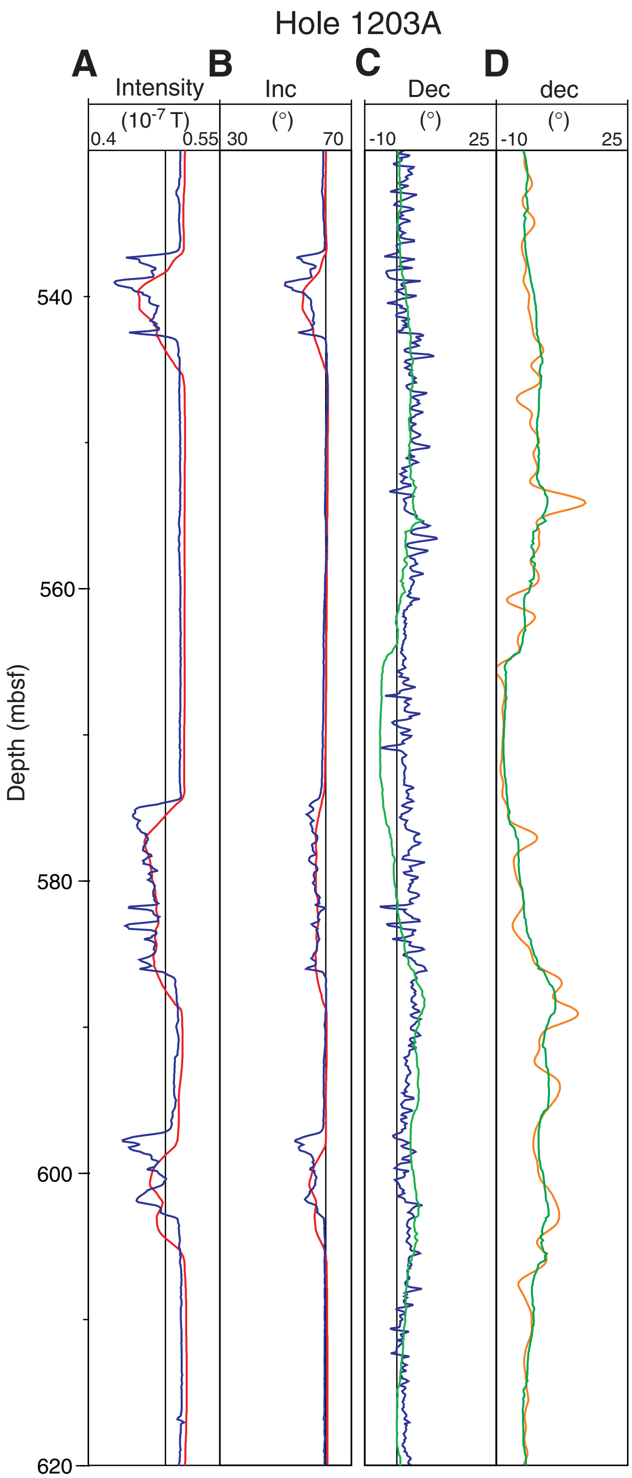

Figure F5. Filters (boxcar, cosine, Gaussian, and Hamming) used in this study. **A.** Impulse responses. **B.** Transfer functions.

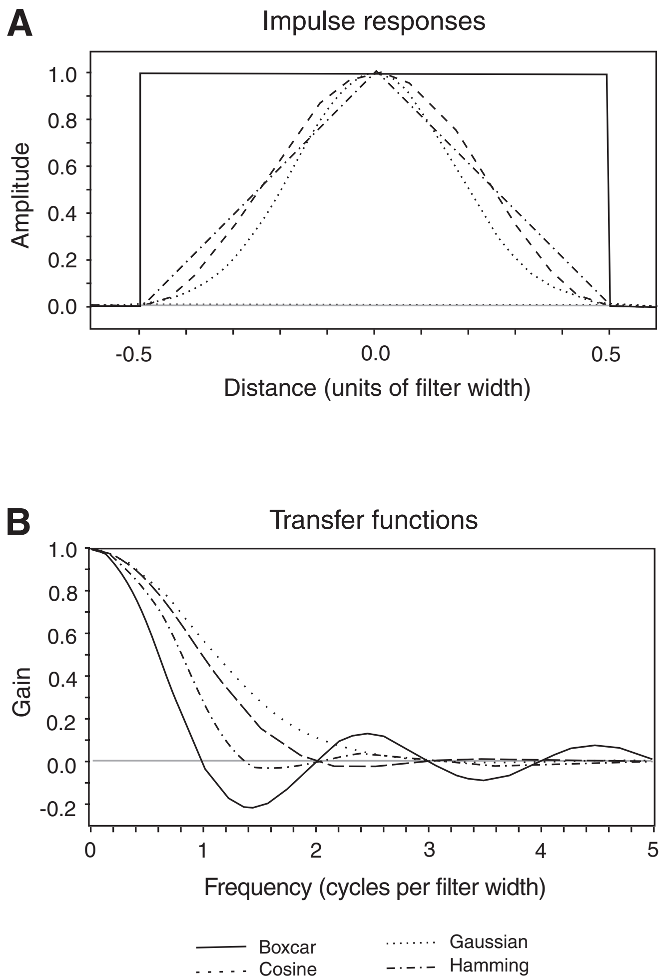

Figure F6. Hole 1203A magnetic logs from the FMS-sonic tool string. **A.** Intensity (F). **B.** Inclination (Inc) of the total magnetic field. **C.** Tool declination (tdec) for pass 1 (gray) and pass 2 (black). **D.** Hole shape: comparison of the Schlumberger algorithm (dark blue; 2.4-m-wide Hamming filter) with the previously validated filtering algorithm (light blue) using (**E**) a 4-m-wide cosine filter and (**G**) a 10-m-wide boxcar filter expressed as residuals (δrot) (**F, H**) between these two determinations of the tool orientation (rot) component.

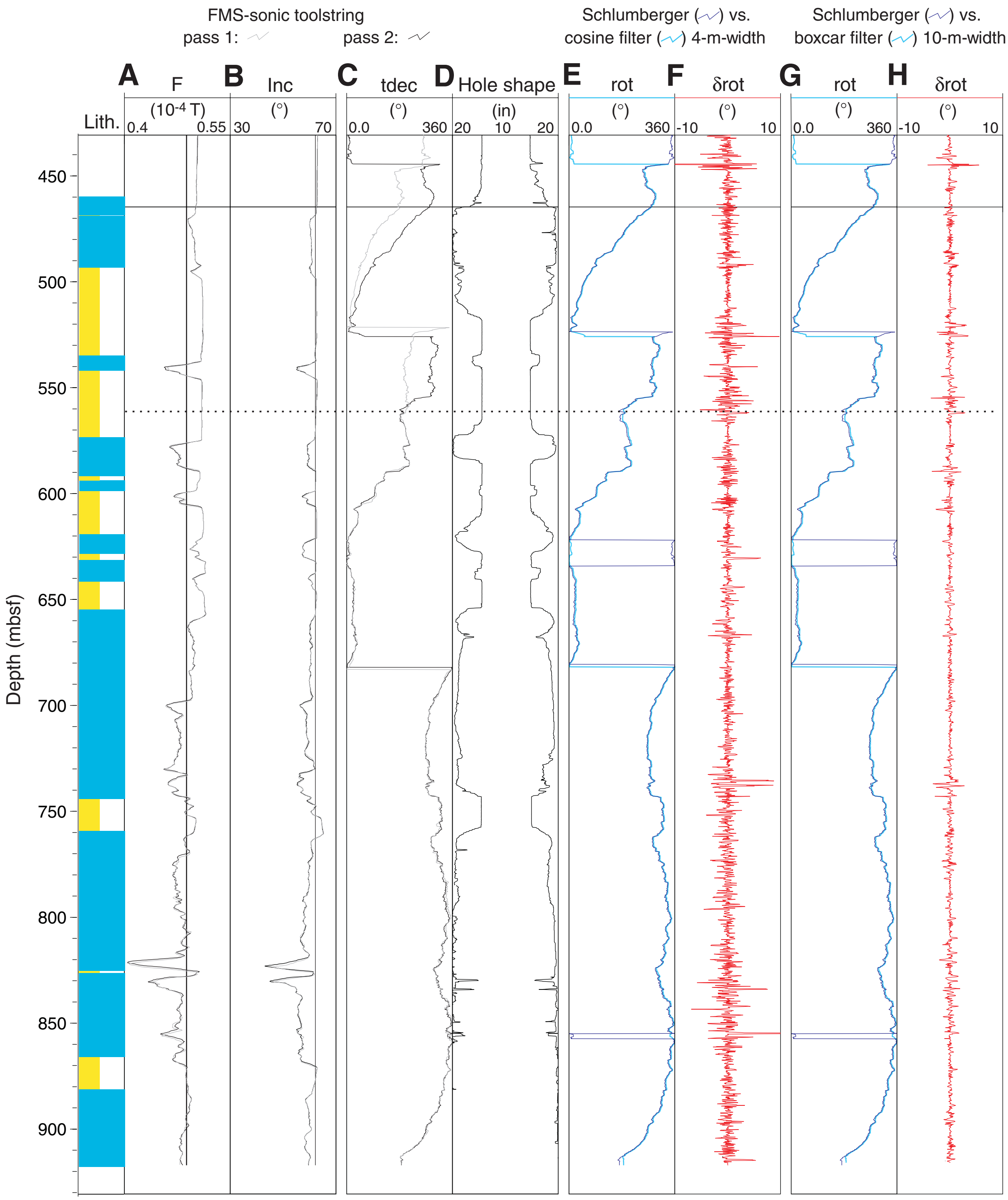

Figure F7. Hole 735B magnetic logs acquired during Legs 118 and 176. **A.** Lithologic units and lithostratigraphy from Dick, Natland, Miller, et al. (1999). **B.** Core magnetic susceptibility (MS) measured by multisensor track (0–450 mbsf; dots) and USGS susceptibility probe MS. **C.** Intensity (F). **D.** Inclination (Inc) of the total magnetic field. **E.** Tool declination (tdec) from the lithodensity tool string (Leg 118; red), Dual Laterolog (Leg 176; green), and FMS-sonic (Leg 176; blue). **F–H.** Comparison of the Schlumberger algorithm (dark color; 2.4-m Hamming filter) with the previously validated filtering algorithm (4-m-wide cosine filter, light color) is shown for the three tool strings (trot = tool rotation).

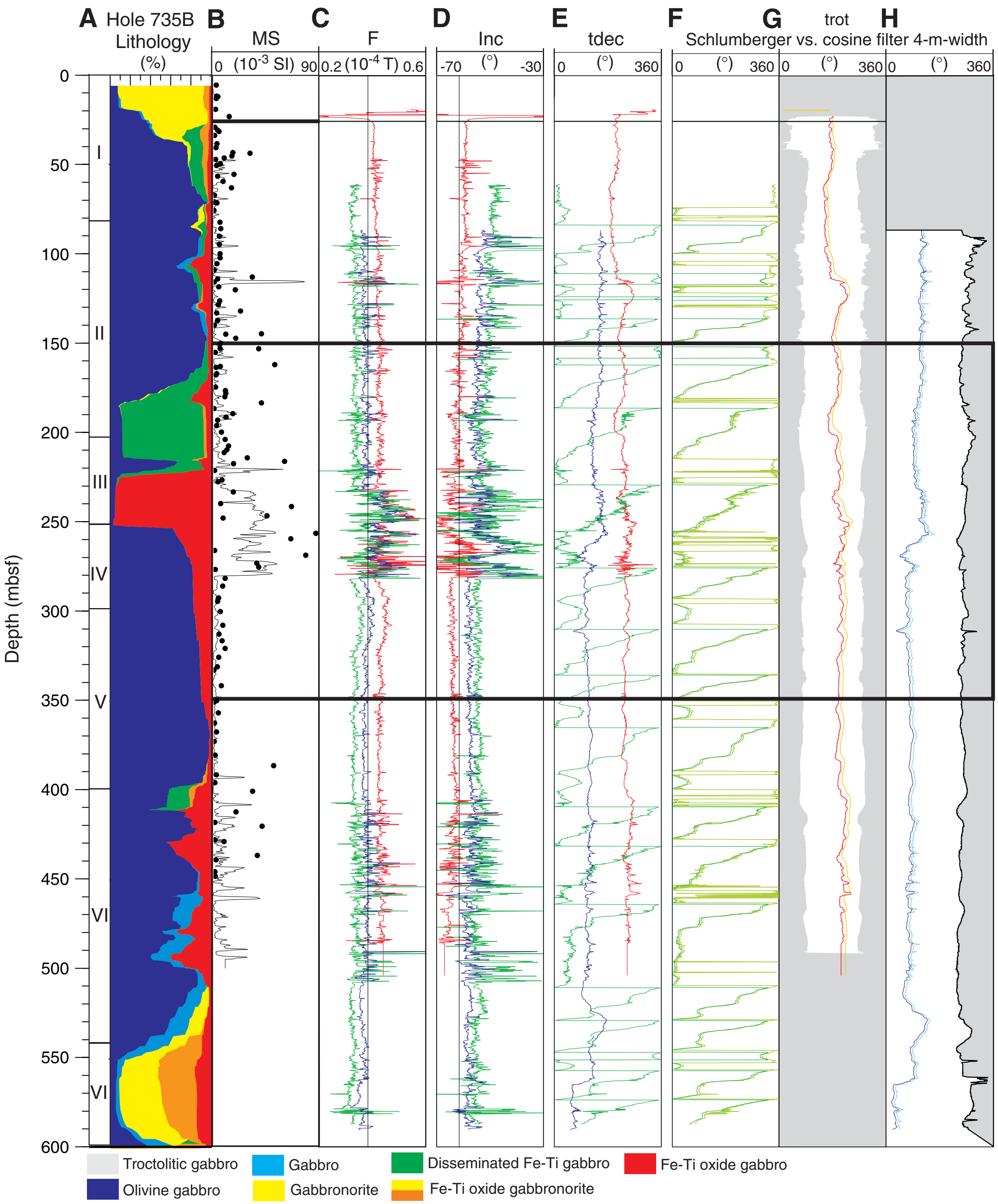

Figure F8. Estimation of filtering quality in Hole 735B: comparison of (**A–C**) oxide-rich layers effects on the declination of the total field with (**D–E**) oxide-rich layer indicators. The difference between the declination (dec = tdec – rot) computed from tool declination (tdec) by removing tool rotation (rot) with the theoretical value for this site (Dec = –61.5°) is plotted for the (A) lithodensity tool string (LDT) (Leg 118; red); (B) dual laterolog (DLL) (Leg 176; green); and (C) FMS-sonic (Leg 176; blue). As an intrinsic property of the formation, similar values are expected and must correlate with oxide-rich layer indicators such as formation (D) magnetic susceptibility (MS) and (E) electrical resistivity.

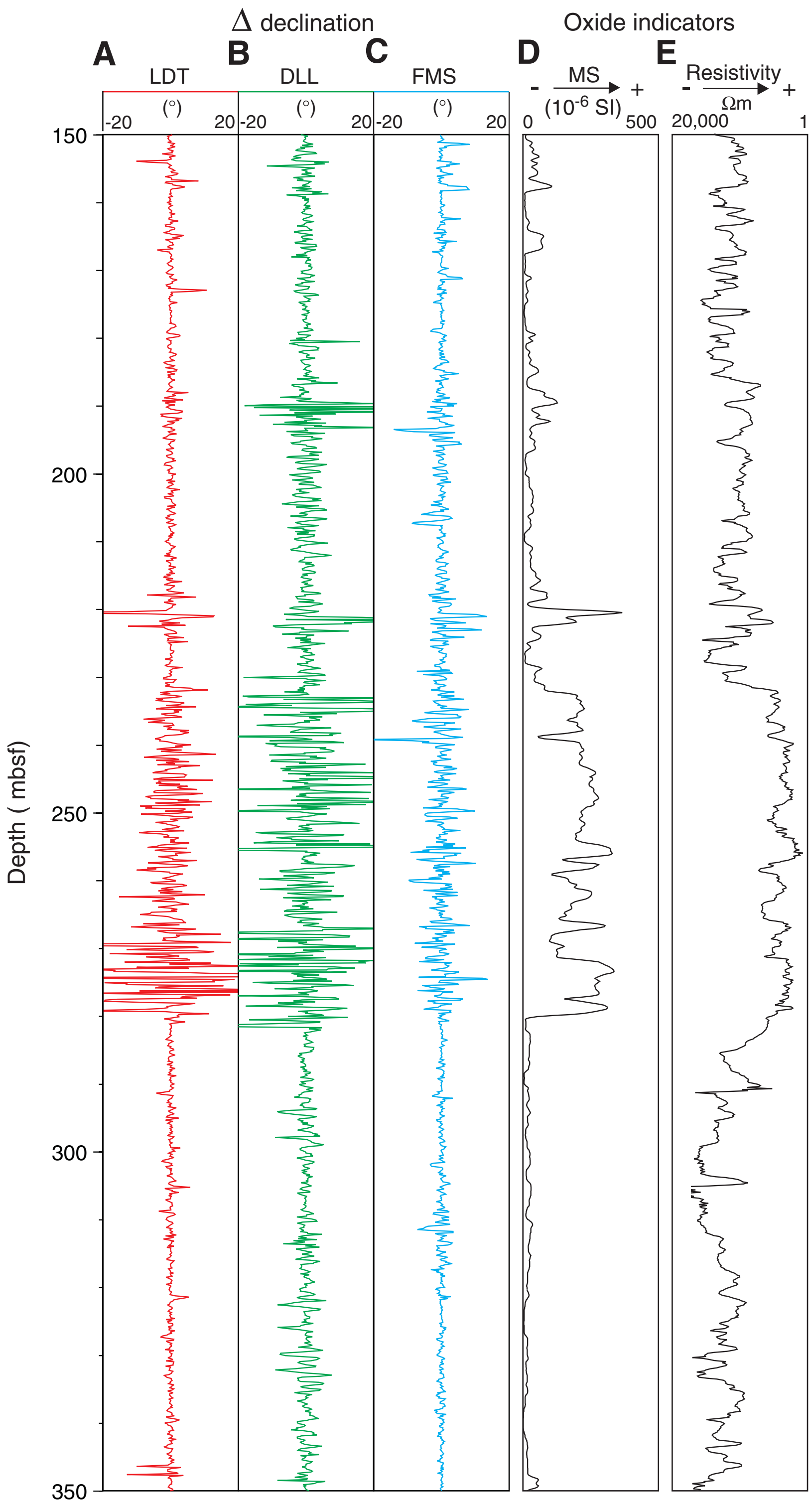

Table T1. Notation.

Parameter	Definition and comments
F	Intensity of the local magnetic field
DEC	Tabulated declination at the site under study
Inc	Inclination of the local magnetic field
FNOR*	Filtered version of F using the Schlumberger algorithm
FINC*	Filtered version of Inc using the Schlumberger algorithm
P1AZ*	Tool orientation determined by the Schlumberger algorithm
Dec	Direct declination measured by the oriented GBM magnetometer
Rot	Direct GBM rotation measured by its gyroscopic system; optical-gyro-based tool orientation
Fx, Fy, Fz	Intensity of the local magnetic field measured by a three-axis magnetometer (GBM or GPI)
tdec	Declination computed from the raw magnetic measurements (Fx, Fy, and Fz). This measurement is made in the tool frame in respect to the x-axis. It integrates both the true local value of the declination and the rotation component of the tool. If the true local value (measurement) is different than that of the tabulated declination (DEC), the orientation of the tool is incorrect. For sub-vertical boreholes, tdec = arctan (Fy/Fx).
rot	Indirect tool rotation obtained by keeping the low-frequency component of tdec magnetometer-based orientation
dec	Local declination obtained by keeping the high-frequency component of tdec
Drot	Local difference between Rot and rot determined using the newly developed algorithm
drot	Local difference between rot determined using the developed algorithm and rot determined using the Schlumberger algorithm
Ddec	Local difference between Dec and dec

Notes: * = Schlumberger acronym. GBM = Göttingen Borehole Magnetometer, GPI = general-purpose inclinometry module.